

Structural changes in amber due to uranium mineralization



Martina Havelcová^{a,*}, Vladimír Machovič^{a,b}, Jiří Mizera^{c,a}, Ivana Sýkorová^a, Miloš René^a, Lenka Borecká^a, Ladislav Lapčák^b, Olga Bičáková^a, Oldřich Janeček^d, Zdeněk Dvořák^d

^a Institute of Rock Structure and Mechanics, AS CR, V Holešovičkách 41, 182 09 Praha 8, Czech Republic

^b Institute of Chemical Technology Prague, Technická 5, 166 28 Praha 6, Czech Republic

^c Nuclear Physics Institute, AS CR, Hlavní 130, 250 68 Řež, Czech Republic

^d Severočeské doly, a.s., Doly Bílina (North Bohemian Mines, Bílina Mines), 5. května 213, 418 29 Bílina, Czech Republic

ARTICLE INFO

Article history:

Received 18 November 2015

Received in revised form

30 March 2016

Accepted 4 April 2016

Keywords:

Fossil resin

Amber

Uranium

Radiolytic alteration

Micro-FTIR

Mapping

SEM/EDX

ABSTRACT

The presence of uranium, with a bulk mass fraction of about 1.5 wt% and radiolytic alterations are a feature of Cenomanian amber from Křížany, at the northeastern edge of the North Bohemian Cretaceous uranium ore district. Pores and microcracks in the amber were filled with a mineral admixture, mainly in the form of Zr-Y-REE enriched uraninite. As a result of radiolytic alterations due to the presence of uranium, structural changes were observed in the Křížany amber in comparison with a reference amber from Nové Strašecí in central Bohemia; this was of similar age and botanical origin but did not contain elevated levels of uranium. Structural changes involved an increase in aromaticity due to dehydroaromatization of aliphatic cyclic hydrocarbons, loss of oxygen functional groups, an increase in the degree of polymerization, crosslinking of C–C bonds, formation of a three-dimensional hydrocarbon network in the bulk organic matrix, and carbonization of the organic matrix around the uraninite infill.

© 2016 Elsevier Ltd. All rights reserved.

1. Introduction

In organic geochemistry, the interaction of ionizing radiation with natural organic matter is an interesting phenomenon that should be studied for several reasons, and can be viewed from various standpoints. The energy transferred by ionizing radiation to organic matter can induce a complex series of reactions generating and altering organic matter in various environments. Vice versa, the organic matter plays an important role in the transport, accumulation and hydrothermal mineralization of uranium and thorium in sediments, and it is also a sensitive marker allowing characterization of the paleoenvironmental, geochemical, and diagenetic history of sediments. Processing of organic matter also takes place in extraterrestrial environments such as cometary and interstellar ices and planetary atmospheres, and must have represented an important process of prebiotic organic evolution on the early Earth (Court et al., 2006; Landais, 1996).

The radiolytic alteration of organic assemblages has been studied by analysis of organic matter present in various forms (usually as bitumens and kerogens) and amounts in uranium and thorium sedimentary deposits (e.g., Court et al., 2006; Kříbek et al., 1999; Landais, 1996; McCready et al., 2003; Sangély et al., 2007). Fixation of uranium by coal, and the influence of uranium on the structural transformation of coal organic matter, has also been studied (e.g., Havelcová et al., 2014b; Meunier et al., 1990; Nakashima et al., 1984). The main alterations in organic matter, which take place in the presence of uranium, are oxidation, biodegradation, radiolysis, and thermal degradation. Complexation and redox reactions are two main processes involved in uranium ore formation, promoted by the presence of organic matter. During thermal treatment, soluble U(VI) species, including organic uranyl complexes, can be reduced to insoluble U(IV) species (Landais, 1996).

Court et al. (2006) summarized the effects of radiolytic alteration of organic matter, as reported previously in the literature: *i*) enrichment in ¹³C; *ii*) greater aromaticity; *iii*) decreased degree of alkylation of polyaromatic hydrocarbons; *iv*) decreased pyrolysis and yields of solvent extracts; *v*) greater structural disorganisation;

* Corresponding author.

E-mail address: havelcova@irms.cas.cz (M. Havelcová).

vi) lower H/C and higher O/C ratios; vii) increased hardness and reflectance; viii) increased thermal maturity, as indicated by an elevated Rock-Eval peak pyrolysis temperature. Based on experimental data obtained on a set of naturally occurring organic assemblages, the authors further concluded that the radiolytic modification of hydrocarbon complex mixtures proceeds via cleavage, aromatization and oxidation, and by transforming aliphatic hydrocarbons into aromatic hydrocarbons. In the pyrolysis products of the complex hydrocarbon mixture, a decrease in the average size and degree of alkylation of polycyclic aromatic hydrocarbons caused by irradiation, as well as enrichment in ^{13}C , was observed. Radiolysis of water produces hydroxyl radicals, whose reactions increase the degree of oxidation due to the formation of phenols, aromatic ketones, aldehydes, and carboxylic acids (Court et al., 2006).

Radiolysis is a spatially localized process and thus the interpretation of analytical data obtained in a larger or even bulk rock sample is difficult. The radiation dose absorbed by organic matter is imparted only to the mass of material within reach of the emitted particles, i.e., mainly alpha particles in the case of uranium and thorium decay. Their effective range in organic matter, within which the particles have sufficient energy to alter the material, has been estimated to be 50 μm (Sangély et al., 2007). In coal, e.g., a local increase in the degree of coalification and iso- or anisotropic haloes around mineral grains and along cracks filled with minerals is typical for radiolytic alteration (Taylor et al., 1998).

Decay of uranium and thorium can induce radiolytic polymerization of light hydrocarbons such as methane, and the formation of complex polyaromatic hydrocarbons (Court et al., 2006). Through radiation-induced polymerization of liquid and/or gaseous pyrolysates, thoriferous and uraniferous bitumen nodules in Phanerozoic sandstones were formed. In these, alpha particles caused the rupture of bonds and formation of free radicals by removing hydrogen, and subsequent crosslinking as new C–C bonds formed a three-dimensional network of hydrocarbons. The molecular weight increased and the materials quickly became insoluble (McCready et al., 2003).

The present work is, to our knowledge, the first report of uranium mineralization in a fossil plant (tree) resin - amber. The ability of some resins to fossilize and to be preserved in the geological record is a fascinating aspect. The main process in fossilisation of resins and formation of amber is polymerization of terpenoid compounds that form the general polymeric structure. Because resin is a mixture of compounds, fossil resins are not completely consistent heteropolymers. Moreover, some terpenoids are non-polymerisable, and they stay protected in the fossilized polymer structure. Polymerizability depends on the molecular structure of terpenoids. Mainly the conjugated diene in terpenoid acids (labdane skeletal type) enables polymerization and, hence, formation of amber. Other terpenes, for example, abietic and pimaric acids, the most abundant components in resins of Pinaceae, remain due to their skeleton being unpolymerized. High pressure, heat, bacterial processes, and the strength of mineral crystallization cause oxygen deprivation and displacement of resinous substances into cracks in the fossilized wood matter and beyond. Individual tree species produce different types of resins; however, not all types of resins can fossilize. The fresh natural resin must be resistant to decay. The resin, sealed and preserved in rocks, changes its structure over time with the formation of complex compounds of higher molecular weight and conversion of volatile and reactive components into stable compounds. This leads to curing of the resin. This process is slow and depends on complex geological conditions, including composition of the original resin. Resin can fossilize as either a precipitated product of tree bark, or in a non-excluded form inside the tree. "Amber" is a term that refers to materials derived from

biological matter that is incorporated into sediments. In anaerobic environments, e.g., during formation of a peat swamp and particularly during coal formation, the resin is concentrated and its mass can increase. Despite chemical alteration during diagenesis, biomarkers still have the characteristic basic skeletal structures of their precursors in natural resins, and can thus be used as chemosystematic markers (Langenheim, 2003; Otto et al., 2002).

In the present work, the structure of a sample of uranium-rich Cretaceous (Cenomanian) amber from Křizany, at the north-eastern edge of the North Bohemian Cretaceous uranium ore district, was studied using various techniques: elemental, micropetrographic, and thermal analyses, optical and electron microscopy, infrared spectroscopy and microspectroscopy, gas chromatography with mass spectroscopy detection (GC/MS), and analytical pyrolysis (Py-GC/MS). An amber sample of Cenomanian age from Nové Strašecí, with a low uranium content, was analysed as a reference sample.

The study was aimed at identifying and interpreting changes in the polymeric structure of fossil resins due to radiolytic and chemical alterations that probably occurred in the presence of local uranium mineralization.

2. Experimental

2.1. Samples and geological setting

A sample of uranium-rich amber of Cretaceous (Cenomanian) age (94–100 Ma) from the Křizany locality in the Czech Republic was studied. The Křizany uranium deposit is located at the north-eastern edge of the North Bohemian Cretaceous uranium ore district (NBCUOD, Fig. 1). The deposit was mined from 1982 to 1990 and was ranked among smaller uranium deposits in the North Bohemian uranium district. The total mine production of low-grade uranium ore (0.07–0.1 wt% U) was 1108 t of U; for comparison, the total uranium production in NBCUOD mined from 1967 to 1996 was 28 046 t (Kafka, 2003).

Two formations - lower freshwater continental and upper marine sediments - form the fully developed Cenomanian sequence. The basement is formed by low metamorphosed metasediments (phyllites and quartzites) and small bodies of Upper Proterozoic and Upper Devonian granitic rocks. Freshwater sediments are developed in depressions of the paleorelief and consist of conglomerates, pebbly to fine-grained sandstones, and lacustrine siltstones. All of these rocks are often rich in organic matter (coalified plant detritus). The sediments of marine Cenomanian cover the whole area of NBCUOD. The basal part of the marine Cenomanian sediments is formed by washout non-graded, wave-cut and beach sediments, and their upper part by shallow marine sandstones. Uranium mineralization developed in the basal part of the Cenomanian formation, and is divided into four ore horizons according to their stratigraphical positions: The A horizon occurs in the freshwater stream and lacustrine sandstones, the main B horizon occurs at the base of marine Cenomanian in wash-out, fine-grained sandstones and siltstones, and C and D horizons are found in friable sandstones and the uppermost Cenomanian fucoidal sandstones. The main shapes of the ore bodies are plates and lenses, mostly horizontal. The area of the ore bodies exceeded their thickness, varying from decimetres to several metres, by many fold. The mineral assemblage and geochemical composition in the sandstone-hosted infiltration-type uranium mineralization occurring in NBCUOD is diversiform and unique (Čadek et al., 1975; Scharm et al., 1980; Smetana et al., 2002; Sulovský, 2005). Uraninite, complex U-containing gels, hydrozircon, baddeleyite, and U–Th–Ca phosphates (ningyoite, brockite) are the main carriers of uranium. In the whole NBCUOD, four main mineral types have been

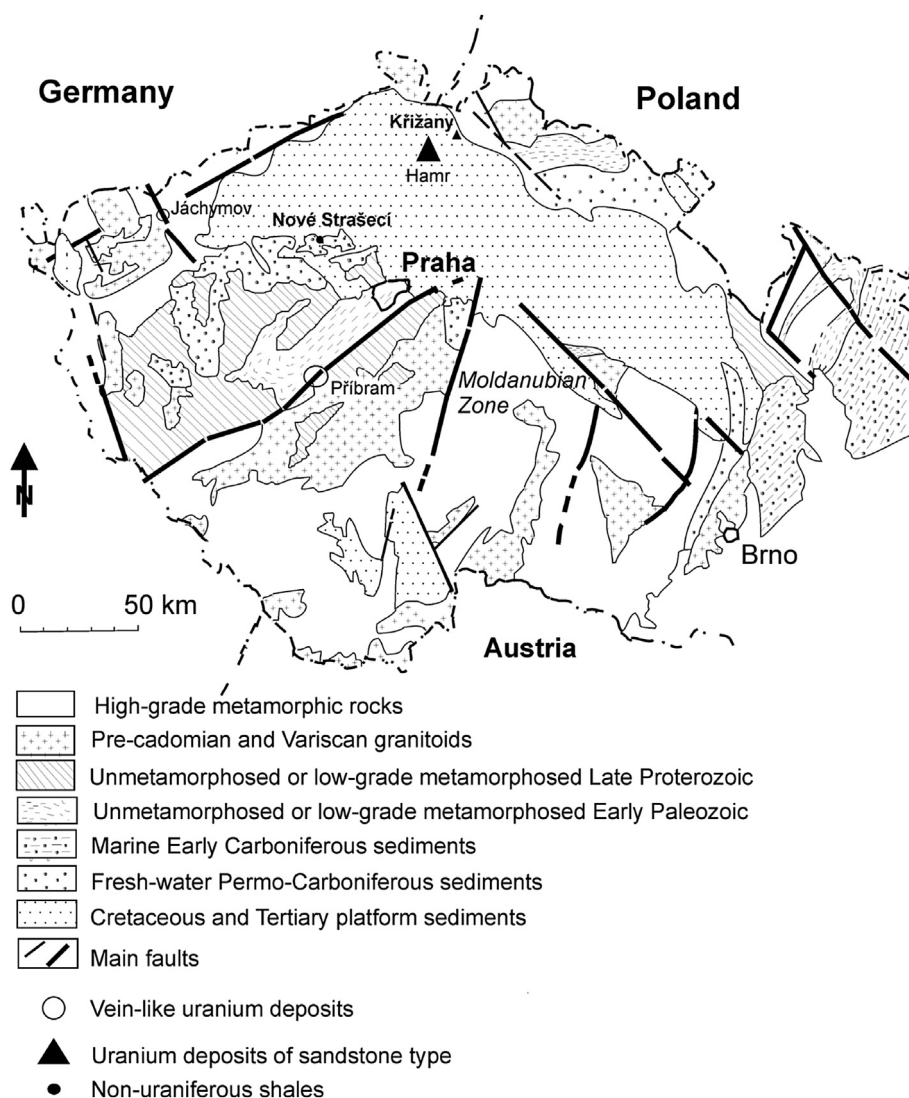


Fig. 1. Schematic geological map of the Czech Republic showing locations of uranium deposits including the location of the Křižany amber (after Kříbek, 1989; modified). The non-uraniferous site, Nové Strašecí, where a reference low-uranium amber was sampled, is also shown.

recognised: uraninite-hydrozircon, uraninite, hydrozircon, and uraninite-ningyoite. A general feature of all uranium ore types is the presence of rare earth elements (REE) and Y, both as admixtures in authigenic minerals (hydrozircon, uraninite, ningyoite, and brockite) and as proper REE or Y minerals (crandallite group, chernovite-(Y), rhabdophane group, and synchysite) (Scharmová and Scharm, 1994; Sulovský, 2005).

The amber sample was found in non-graded, fine- to medium-grained sandstones with a high content of irregular shaped quartz grains, sized 1–3 cm. These sandstones are part of basal marine Cenomanian sediments (uranium ore horizon B). Amber occurred in these sandstones as big loaf-shaped bulbs, 10–20 cm in size. Freshly excavated amber had a honey-like, yellow, orange, light brown or red-brown colour, and was translucent-to-transparent, which changed after several months to a dark brown, opaque colour.

As a reference, amber formed in roughly the same epoch and under similar conditions, but in the absence of uranium mineralization, a sample of the Cenomanian age from Nové Strašecí (see Fig. 1) was analysed. This sample was chosen not only due to a similar age and location, relatively close to Křižany (about 100 km),

but also due to an identical or very similar botanical origin of both fossil resins (Havelcová et al., 2014a). The sample was found in an operating surface mine, where Carboniferous refractory clays belonging to the Kladno Formation are mined. The amber occurred within a layer of dark clays with plentiful charred plant remains, which were formed in the area of littoral peat-bogs with abundant halophytic (salt-tolerant) vegetation. It was present in the form of tiny spheres and cylinders (size of 2–3 mm, rarely up to 1.5 cm), pale yellow (almost colourless) to yellow, and, after ageing for several months, changed to a brown, partly transparent colour.

2.2. Instrumentation

The elemental organic composition of the amber samples was determined using a Flash FA 1112 (Thermo Finnigan) CHNS/O micro-analyzer.

Several major and trace elements were assayed by instrumental neutron activation analyses (INAA). Irradiations for INAA were carried out in the LVR-15 experimental nuclear reactor of the Řež Research Centre within the CANAM infrastructure (project No. LM2011019 of the Ministry of Education, Youth and Sports of the

Czech Republic). Detailed descriptions and discussions of the analytical procedures can be found in, e.g., Mizera and Řanda (2010) and Řanda et al. (2007). Unfortunately, a high uranium content in the Křižany amber hindered assaying major elements such as Al, Mg, Ca, and Ti using the short time irradiation mode of INAA, and even in the long time irradiation mode, determination of some elements was hindered by interference from the neutron-induced fission of uranium.

Microchemical analysis using environmental scanning electron microscopy (ESEM-EDX) employed a Philips XL30 ESEM FEI electron microscope equipped with electron detectors, SED (GSED) for micromorphology and BSED (GBSED) for phase contrast, both in high vacuum and environmental modes. The microprobe analyses of uraninite were performed using a Cameca SX-100 microprobe in the WDX mode.

Micropetrography of amber was studied on particulate polished sections using an Olympus BX51 and a Carl Zeiss Axio Imager M2m microscopes for reflected light, and procedures according to the standards of the International Organization for Standardization (ISO 7404), Sýkorová et al. (2005), and Taylor et al. (1998). The composition of lipinitite macerals was checked in fluorescence mode according to Taylor et al. (1998) and ISO 7404.

Thermogravimetric and differential thermogravimetric analyses (TGA and DTG, respectively) employed a Perkin Elmer TGA 6 analyzer. The analyses were carried out under a nitrogen atmosphere at a heating rate of $10\text{ }^{\circ}\text{C min}^{-1}$. Kinetic data were evaluated using Perkin Elmer Pyris™ software, version 5.0.

Fourier transform infrared (FTIR) spectra of the bulk samples were collected on a Nicolet 6700 FTIR spectrometer (Thermo Nicolet Instruments Co.) with a N_2 purging system. Spectra were acquired using a single reflection ATR (Attenuated Total Reflection) SmartOrbit accessory equipped with a single bounce diamond crystal (angle of incidence 45°). Each sample spectrum averaged 64 scans and the resolution was 2 cm^{-1} . The spectra were ratioed against a single-beam spectrum of the clean ATR crystal and converted into absorbance units by ATR correction. Data were collected over a wavenumber range $4000\text{--}400\text{ cm}^{-1}$.

Micro-ATR FTIR analysis (ATR mapping) employed a Nicolet 6700 spectrometer combined with a Thermo Continuum IR microscope. The system is equipped with a X–Y–Z motorised stage with incremental steps of $1\text{ }\mu\text{m}$. A polished section was placed on the microscope stage and the area of investigation ($700 \times 500\text{ }\mu\text{m}$) was selected through a $15 \times$ objective. Spectra were acquired over a wavenumber range of $4000\text{--}650\text{ cm}^{-1}$, from 64 scans, at a spectral resolution of 4 cm^{-1} . An ATR germanium crystal directly connected to the objective was used, resulting in investigated areas of about $40 \times 40\text{ }\mu\text{m}$. A step size of $30 \times 20\text{ }\mu\text{m}$ was used (640 points were measured). Data collection and post-run processing were carried out using Nicolet Omnic ATR imaging software.

For GC/MS analysis, amber samples were sonicated with dichloromethane. The extracts were analysed using a Trace Ultra - DSQ II (Thermo Scientific) instrument equipped with a capillary column TR-5MS. The GC oven was heated from $37\text{ }^{\circ}\text{C}$ (3 min) to $100\text{ }^{\circ}\text{C}$ at a rate of $10\text{ }^{\circ}\text{C/min}$ and then to $300\text{ }^{\circ}\text{C}$ (8 min) at a rate of $10\text{ }^{\circ}\text{C/min}$. As an internal calibration standard, 5- α (H)-androstanone in iso-octane was used. TMAH-Py-GC/MS analyses were performed using a CDS Pyroprobe 5150 pyrolysis unit (CDS Analytical) connected to the above GC/MS instrument. Samples of powdered amber, together with $10\text{ }\mu\text{L}$ of a 25 wt% aqueous solution of TMAH (tetramethylammonium hydroxide) for methylation trials, were heated at $610\text{ }^{\circ}\text{C}$ for 30 s. The Py-GC interface was kept at the maximum allowed temperature of $300\text{ }^{\circ}\text{C}$. The TR-5MS column was used and the temperature program of the columns was set from 35 to $300\text{ }^{\circ}\text{C}$ at a rate of $5\text{ }^{\circ}\text{C/min}$. Identification of compounds was based on comparison of spectra with the NIST/EPA/NIH Mass

Spectral Library or with literature data (Philp, 1985).

3. Results

3.1. Micropetrographic and elemental analyses

Petrographical characteristics (maceral composition) and the basic organic elemental (CHNS–O) composition of the fossil resins are presented in Table 1. The contents of several major and trace elements, mainly characterizing the mineral phase of the resins, are presented in Table 2.

The Křižany amber mainly contained resinite (maceral of lipinitite group) with remnants of coalified wood tissue that has been classified as huminite and its macerals – ungelified textinite and gelified ulminite with a random reflectance $R_r = 0.24\%$ (Table 1). Large differences were observed in the morphologies and optical properties of both resinite and ulminite, probably caused by uneven radiolytic alterations. In normal light, resinite is a brown material with a homogeneous, slightly porous to fine-grained texture, with a reflectance value of about 0.10%. Around cracks filled with uranium-bearing minerals, and in dispersed sub-microscopic intermixtures with uranium, resinite changed to grey coloured matter with a reflectance of 0.17%, up to white haloes with reflectance reaching 0.35% (Fig. 2A,C). In blue light, resinite had a bright yellow fluorescence colour that diminished with increasing radiolytic alteration and changed to dull brown or black in the haloes (Fig. 2B). Bright zones also appeared along cracks in the huminite. The reflectance of altered ulminite increased from 0.24% to 0.37% in bright haloes and zones along cracks and fissures (Fig. 2D).

A sample of fossil resin from Nové Strašecí was also mainly resinite, with a rare admixture of huminite particles, named corpopohuminitite (Table 1 and Fig. 3C). Resinite, with a reflectance value of 0.15%, had a bright yellow fluorescence colour. Numerous darker cracks and hems caused by weathering occurred at the edges of resinite grains (altered resinite in Table 1), which rarely contained fine-grained inorganic material (Fig. 3A,B). Rare formations of corpopohuminitite ($R_r = 0.25\%$) were identified as a rest of cork tissue hemming resinite formations (Fig. 3C,D).

The elemental composition of the Křižany amber (Table 2), besides the anomalous enrichment in U, also showed high levels of other elements, especially Fe and Zn. Compared to the amber from Nové Strašecí, most elements were substantially higher in the Křižany amber, probably reflecting a higher mineral component.

3.2. Composition of uraninite in the Křižany amber

Some cracks occurring in the amber from Křižany were filled with uraninite (Fig. 4). Microprobe analysis shows that uraninite displayed anomalous enrichment in Zr (up to 4.97 wt% ZrO_2 , see Table 3). The anomalous enrichment in Zr in the examined uraninite is unique in comparison with worldwide uraninite occurrences and ore deposits. This enrichment was highly correlated with unique U–Zr–REE mineralization occurring in NBCUOD (Čadek et al., 1975; Scharm et al., 1980; Sulovský, 2005). Similar, but distinctly lower Zr concentrations were found in uraninite from partially similar roll type uranium deposits on the Colorado Plateau (up to 0.93 wt% ZrO_2 ; Zhao and Ewing, 2000). Zirconium enriched uraninite also occurred in Egypt, in a hydrothermal ore deposit associated with high-K calc-alkaline granites (up to 2.49 wt% ZrO_2 ; Shahin, 2014). Low totals of all analyses of uraninite in the Křižany amber (see Table 3) could be due to hydration and oxidation of uraninite, similar to an interpretation by Zhao and Ewing (2000) for uraninite from the Colorado Plateau.

Table 1
Basic petrographic and elemental characterization of amber samples.

Sample	Maceral composition	C ^a	H ^a	N ^a	S ^a	O ^a	H/C ^b	O/C ^b	SOM ^c
Křížany	Liptinite: 96.5 vol% (82.7 vol% resinite-liptodetrinite-bituminite, 13.8 vol% altered liptinite) Huminitite: 3.5 vol% (0.5 vol% textinite, 1.5 vol% ulminite, 1.5 vol% altered ulminite)	85.5	10.8	2.1	0.7	1.0	1.51	0.01	1.2
Nové Strašecí	Liptinite: 98.2 vol% (92.0 vol% resinite, 6.2 vol% altered resinite) Huminitite: 1.8 vol% (corpohuminitite)	76.7	10.1	1.9	0.1	11.2	1.58	0.11	9.8

^a wt.%, dry matter.^b Atomic ratio.^c SOM - soluble organic matter, wt.%.**Table 2**
Elemental composition of amber samples obtained by INAA (in mg kg⁻¹; n.d. - not determined).

Sample	Na	Sc	Cr	Fe	Co	Zn	As	Br	Sb
Křížany	189	1.42	104	25 498	26.8	4054	360	41.6	11.9
Nové Strašecí	68.6	0.423	3.52	191	0.208	n.d.	5.38	1.23	0.131
Sample	Sm	Eu	Tb	Yb	Hf	Ta	W	Th	U
Křížany	461	0.437	3.90	15.4	9.68	0.548	188	4.23	14 725
Nové Strašecí	8.58	0.092	n.d.	n.d.	n.d.	n.d.	146	n.d.	1.40

Combustion of the amber from Křížany started below 100 °C and the first significant weight loss was observed at 101 °C, corresponding to loss of water adsorbed in the pores. The main peak was located at 430 °C. Similar values were found by [Ragazzi et al. \(2003\)](#) in amber specimens from the Dolomites, Italy, of much older age (Triassic, ~225 Ma). Complete combustion of the sample was not achieved and only 47 wt% was degraded at 500 °C. On the other hand, the combustion profile of the Nové Strašecí amber began at about 250 °C and total combustion of the sample was achieved

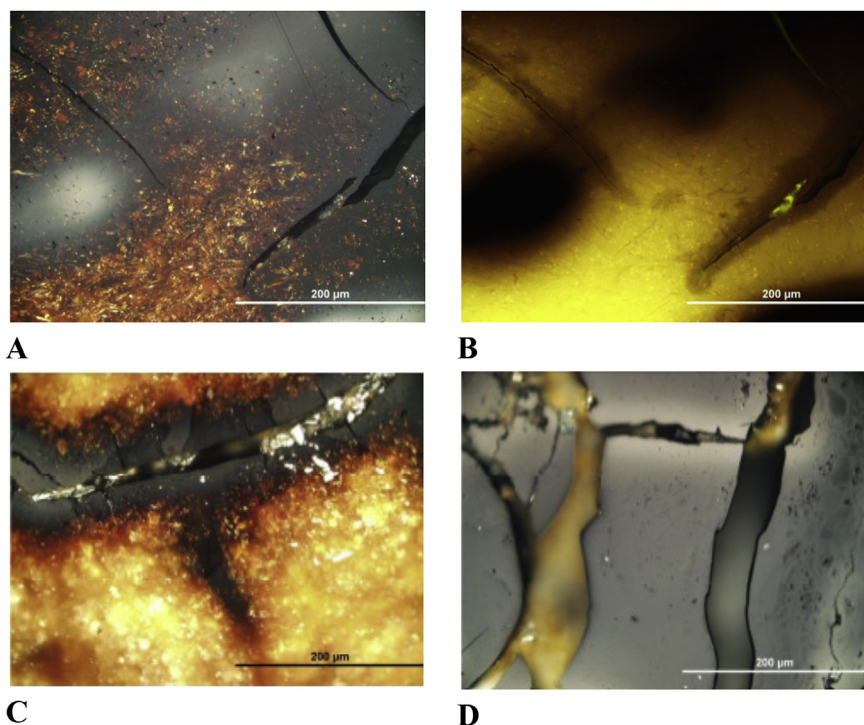


Fig. 2. Micrographs of polished sections on the amber from Křížany. (A) Fissures in unevenly altered resinite with increased reflectance from 0.12% to 0.33%. (B) Yellow fluorescence of unaltered resinite and brown to dark fluorescence of altered resinite. (C) Altered matter along the crack in resinite filled with minerals. (D) Altered ulminite with increased reflectance from 0.26% to 0.37% in white zones along fissures. (For interpretation of the references to colour in this figure legend, the reader is referred to the web version of this article.)

3.3. TGA/DTG measurements

Thermogravimetric and derivative thermogravimetric analyses (TGA and DTG, respectively) have recently been applied in studies of fossil resins to observe the degree of resin polymerization during amberization ([Rodgers and Currie, 1999](#); [Ragazzi et al., 2003](#); [Treviani et al., 2005](#); [Cebulak et al., 2003](#)).

Results of TGA/DTG measurements carried out with the amber samples from Křížany and Nové Strašecí are illustrated in [Fig. 5](#).

below 500 °C. The main peak indicating a maximum rate of weight loss was at 422 °C, which is almost identical to the value of 421 °C found by [Ragazzi et al. \(2003\)](#) in amber from the Raritan Formation, New Jersey, USA, of similar age (Turonian, 94–90 Ma) and elemental composition (C 78.41 wt %, H 10.06 wt%, O 11.24 wt%).

3.4. Infrared spectroscopy

Although the chemical structure of amber is quite complex and

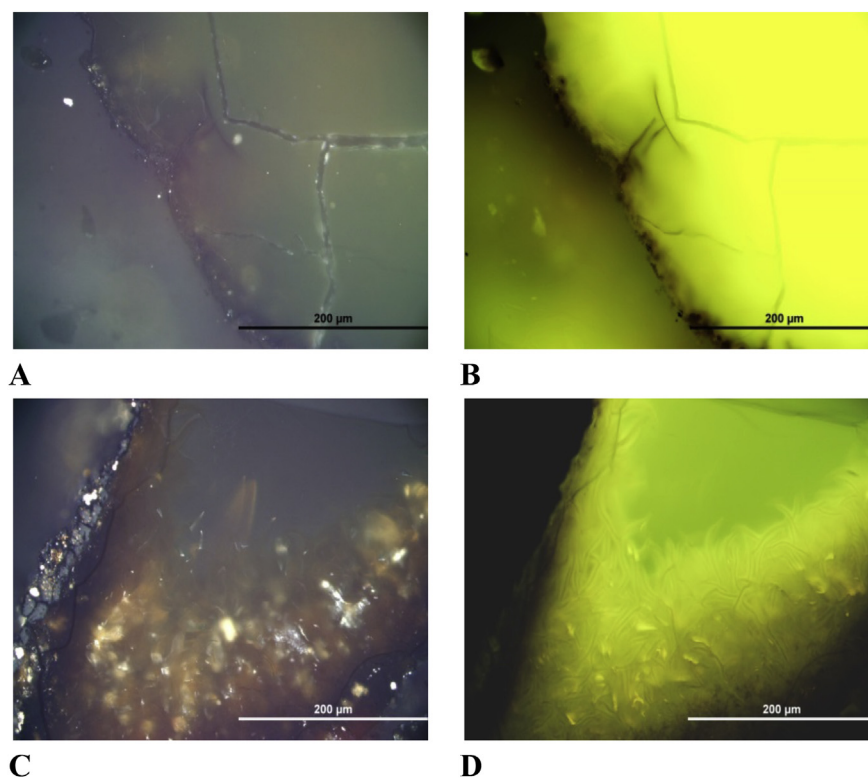


Fig. 3. Micrographs of polished sections on the amber from Nové Strašecí. (A) Resinite ($R = 0.15\%$) with cracks. (B) Bright yellow fluorescence of resinite with darker cracks and hems on the edge. (C) Resinite formation with internal cracks and coloured reflexes, hemmed by a grey corpohuminite network. (D) Yellow-green fluorescence of the resinite formation with a dark hem of corpohuminite. (For interpretation of the references to colour in this figure legend, the reader is referred to the web version of this article.)

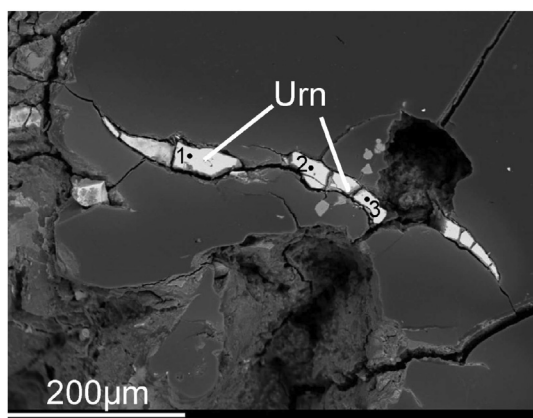


Fig. 4. Back scattered electron micrograph of a crack in the amber from Krížany filled with uraninite. The numbered points indicate locations where the microprobe analyses was performed (see the results in Table 3).

Table 3

Results of microprobe analyses of uraninite (wt %) in locations 1, 2, and 3 within a crack in the amber from Krížany (see Fig. 4), and corresponding crystallochemical formulae.

	1	2 wt.%	3		1	2 apfu ^a	3
UO ₂	77.43	85.22	76.40	U	1.63	1.64	1.62
ThO ₂	0.04	0.00	0.13	Si	0.02	0.01	0.02
SiO ₂	0.16	0.10	0.17	P	0.05	0.05	0.06
P ₂ O ₅	0.62	0.72	0.77	Zr	0.23	0.21	0.20
ZrO ₂	4.89	4.97	4.25	Y	0.01	0.00	0.00
Y ₂ O ₃	0.18	0.00	0.00	Ca	0.07	0.06	0.07
Ce ₂ O ₃	0.01	0.03	0.00	Fe	0.03	0.05	0.04
La ₂ O ₃	0.04	0.00	0.01	Mn	0.00	0.00	0.02
CaO	0.72	0.69	0.65	Ti	0.01	0.01	0.02
FeO	0.37	0.63	0.47				
MnO	0.05	0.03	0.11				
TiO ₂	0.08	0.22	0.34				
PbO	0.02	0.17	0.10				
Total	84.61	92.78	83.40				

^a Atoms per formula unit (O = 4).

diverse, there are spectral bands in their infrared (IR) spectra that are clearly distinguishable. These allow fast and non-destructive characterization of the degree of maturation or degradation of an amber sample based on determination of oxygen functional groups and the relative abundance of aliphatic and aromatic structures (Beck et al., 1964). Recent studies often relied on the ATR technique, which does not require special sample preparation for measuring IR spectra. Also IR microspectroscopy is a suitable tool to assess structural zonation of organic phases using the relative abundance of bands of aliphatic and aromatic structures, and carbonyl groups (Sangély et al., 2007). Besides IR spectroscopy, Raman spectroscopy can be utilized for characterization of non-fluorescent fossil resins.

Both spectral methods were successfully applied in structural analysis of valchovite, the Cenomanian amber from Moravia, Czech Republic (Streibl et al., 1976; Vávra, 1993; Jehlička et al., 2004).

The IR spectra of bulk amber samples are shown in Fig. 6. Both spectra were dominated by bands belonging to the anti-symmetric and symmetric stretching vibrations of the aliphatic C–H bonds of methyl, methylene, and methine groups in the wavenumber region 3000–2700 cm⁻¹. In the second derivative of the spectra, six bands were distinguishable at about ~2958 (CH₃), ~2920 (CH₂), ~2895 (CH), ~2865 (CH₃), ~2845 (CH₂), and ~2825 cm⁻¹ (CH₂). The bands of bending vibrations of CH₂ and CH₃ groups were found at 1450 and 1375 cm⁻¹. The presence of aromatic structures was indicated

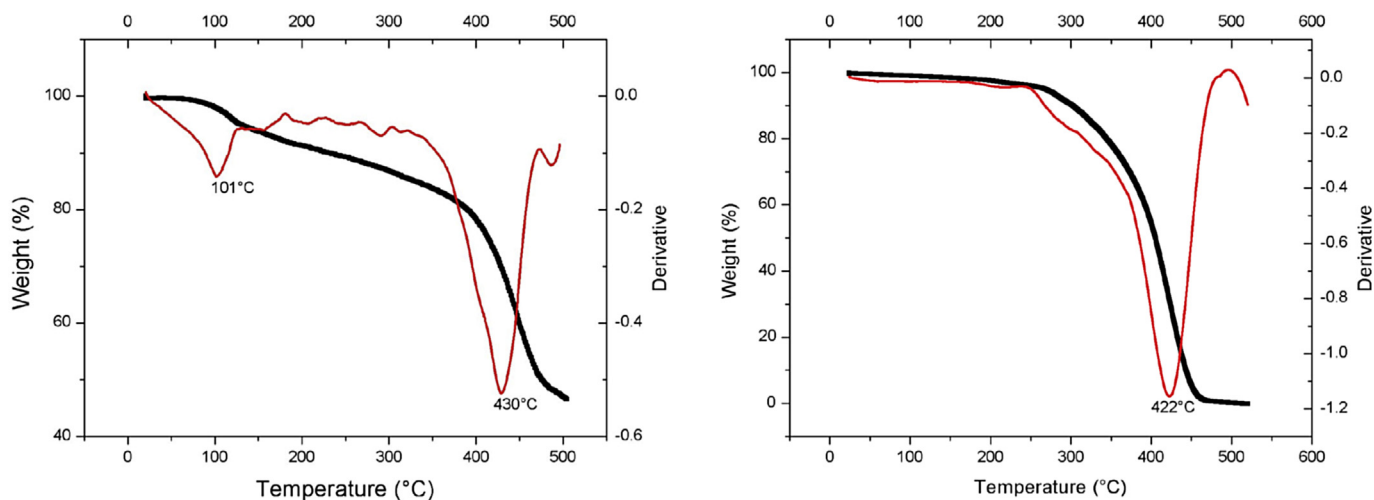


Fig. 5. TGA (thick line) and DTG (thin line) curves of amber samples from Křižany (left) and Nové Strašecí (right).

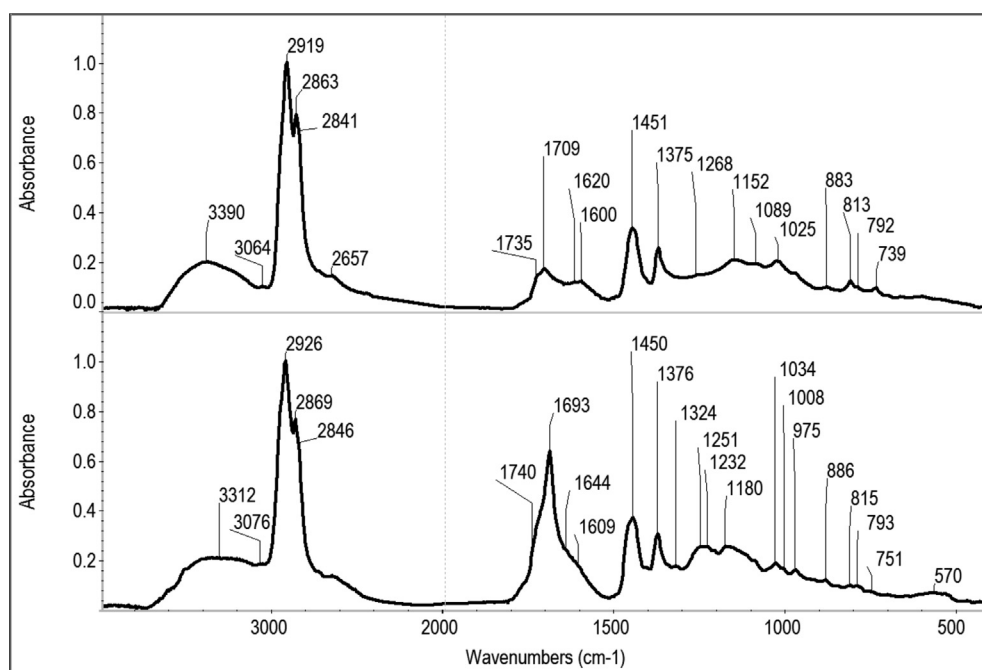


Fig. 6. Infrared spectra of the amber samples from Křižany (upper spectrum) and Nové Strašecí (lower spectrum).

by quite insignificant bands of aromatic stretching vibrations at $3060\text{--}3080\text{ cm}^{-1}$, which overlapped with a stretching vibration band of an exomethylene group ($\nu_{\text{H-C=C}}$). The stretching vibrations of the aromatic ring C=C bond was observed at $\sim 1600\text{ cm}^{-1}$. It follows from comparison of spectra of both amber samples that the Křižany amber contained more aromatic structures. The aromatic character of this sample was also indicated by higher intensities of bands assigned to out-of-plane vibrations of aromatic C-H bonds at $883, 813, 792,$ and 739 cm^{-1} . A low intensity band at 886 cm^{-1} , together with a shoulder at 1644 cm^{-1} in the Nové Strašecí amber, indicated a very low number of exocyclic double bonds in this sample.

The IR spectra also allowed an assessment of oxygen functional groups in both amber samples. Comparing the stretching vibration bands of the C=O bond at $\sim 1700\text{ cm}^{-1}$ in their IR spectra it is clear that the amber from Nové Strašecí had a higher content of carboxyl

groups than the amber from Křižany. Bands at $\sim 1740, \sim 1735,$ and $1709\text{--}1693\text{ cm}^{-1}$ can be assigned to esters, ketones, and carboxyl groups, respectively. The stretching vibration bands of the C-O bond were positioned at $1270\text{--}1200\text{ cm}^{-1}$ in the carboxylic acids. The bands at $1180\text{--}1150\text{ cm}^{-1}$ belong to esters. The abundance of hydroxyl groups was assessed from the intensities of the stretching vibration bands of the O-H bond at $3400\text{--}3300\text{ cm}^{-1}$, but sample humidity contributed to absorption in this region of the spectra. Humidity also contributed to absorption at $\sim 1640\text{ cm}^{-1}$.

3.5. Infrared microspectroscopy

IR microspectroscopy was used to obtain information on structural changes of the organic matter in the Křižany amber as a function of the distance from uranium-containing mineral inclusions. A suitable rectangular area in a polished section of the

amber, with dimensions $700 \times 500 \mu\text{m}$, was chosen for infrared microspectroscopy mapping. This area is depicted on the micrograph in Fig. 7 together with 640 measuring points. Cracks filled with mineral matter containing mainly uraninite are visible clearly in the micrograph.

The IR microspectra were used for calculating a 2D map based on the band intensities of aliphatic C–H bonds of methylene/methyl groups at 2920 cm^{-1} (Fig. 8). In the 2D map, spots with various uranium concentrations measured by SEM/EDX have been marked. Infrared microspectra scanned from individual spots are presented in Fig. 9. The dark areas in the 2D map represent cracks filled with high uranium-containing mineral matter, which causes radiolytic alterations in the amber. In spots with a very low uranium content, the microspectra had very intense bands of aliphatic structures, and the band intensity of aliphatic C–H bonds decreased with increasing uranium concentration, while the relative content of aromatic C=C bonds and oxygen functional groups (RCOOH, RCOR', RCOOR', ROH) increased. A ternary diagram, presented in Fig. 10, illustrates the relative abundance of aliphatic C–H bonds, carbonyl groups, and aromatic C=C bonds due to radiolytic alteration of the Křižany amber. In construction of the diagram, intensities of the bands at 2920 , ~ 1700 , and $\sim 1600 \text{ cm}^{-1}$, respectively, were used. It is obvious that the increase in uranium mass fraction from 0.02 to 0.66 wt% is accompanied by a drastic decrease in aliphatic C–H bonds and a slight increase in carbonyl groups. At higher uranium mass fractions of 12.5 and 28.0 wt%, the aliphatic C–H bonds and oxygen functional groups completely disappeared.

3.6. GC/MS analysis

In the GC/MS (gas chromatography/mass spectrometry) analysis of total extracts of the amber samples, mainly terpenes were identified (Fig. 11). They are diagenetic products (biomarkers) of terpenoids, which are common constituents of resins of higher plants. Concentrations of the identified compounds are shown in

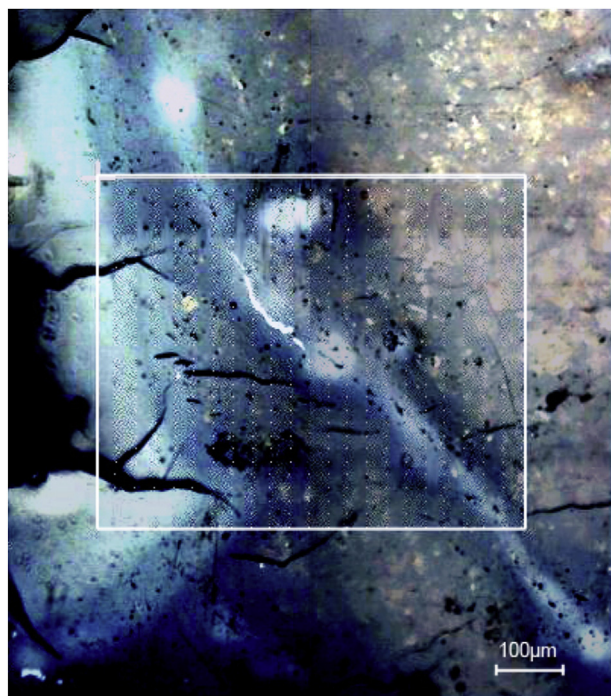


Fig. 7. Micrograph of an area in a polished section from the Křižany amber chosen for infrared microspectroscopy mapping.

Table 4.

The chromatogram of the Nové Strašecí amber extract showed terpenes that are not structurally attached to the polymer matrix. Major components are diterpenoids of the abietane class, typical for conifers. Resins of fossil and extant taxa of Cupressaceae and Taxodiaceae contain diterpenoids of the abietane class, and frequently also phenolic abietanes and some characteristic sesquiterpenoids of cedrane and cuparane classes (von Rudloff et al., 1980; Otto and Wilde, 2001; Otto et al., 2002). Since phenolic abietane (ferruginol) and sesquiterpenoids associated with Cupressaceae and Taxodiaceae are present (cuparene) in the Nové Strašecí amber, its origin from this group of conifers is likely. Cadinene-type compounds (dihydro-ar-curcumene, calamenene) are the most abundant sesquiterpenes, and indicate classification of this amber within Class II, derived from polymers of these bicyclic sesquiterpenoids (Anderson et al., 1992; Langenheim, 2003). These compounds are, however, widely distributed among higher plants and they are not source-specific. The monoterpenoids camphor and borneol were also detected. These compounds are found in higher amounts in resins of angiosperms, but also in lower amounts in resins of gymnosperms. Monoterpenoids predominate in the volatile fraction of the natural resins of many conifers and are not chemotaxonomic source indicators.

In the extract of the Křižany sample, the series of diterpenoid compounds revealed signs of alteration. These compounds are derivatives of abietane and pimarane precursors without conjugated dienes, and thus non-polymerizable. Degradation of amber was also indicated by the presence of an unresolved complex mixture (UCM) in chromatograms. The UCM hump occurs when compounds cannot be resolved and identified by GC. The UCM is thought to be composed of a mixture of constitutional isomers, and linear, branched and cyclic hydrocarbons (Gough and Rowland, 1990).

3.7. TMAH-Py–GC/MS analysis

Characterization of amber and its classification can also be carried out using TMAH-Py–GC/MS (tetramethylammonium hydroxide-pyrolysis-gas chromatography/mass spectrometry). This method is used in order to improve pyrolytic analysis of materials that release polar functional groups. Free carboxylic groups are methylated to their corresponding methyl esters in the presence of TMAH, and separated and detected using GC/MS. The total ion pyrograms from TMAH-Py–GC/MS analysis of amber samples are shown in Fig. 12. The identified peaks are listed in Table 5. The pyrolysates contained terpenes, together with cycloalkanes and cycloalkenes formed by defunctionalization and crosslinking of C–C bonds in the three-dimensional hydrocarbon network. Cycloalkanes and cycloalkenes, which are non-specific markers, were also identified in pyrograms of both amber samples. A significant UCM hump can be noticed in the pyrogram of the uraniumiferous Křižany amber, similar to its extract chromatogram.

4. Discussion

The elemental analysis of a fossil resin (amber) from a uranium deposit in Křižany, at the northeastern edge of the North Bohemian Cretaceous uranium ore district (NBCUOD), revealed an anomalous enrichment in uranium of about 1.5 wt% (see Table 2). Amber is not resistant to structural alteration by geothermal processes, and the radiolytic alteration of amber due to radiation emitted by the uranium decay chain may have played a unique role in changes in the composition and structure of the uraniumiferous Křižany amber. These changes have been observed in comparison with a reference amber sample of similar age and botanical origin, but with a low uranium

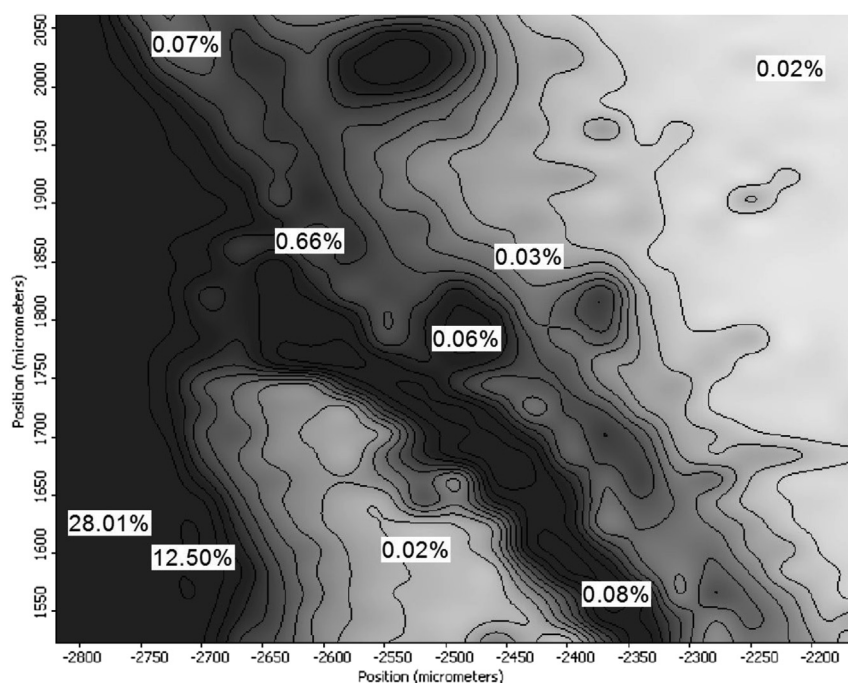


Fig. 8. A 2D band intensity map used for quantification of aliphatic C–H bonds by infrared microspectroscopy on a polished section from the Křižany amber (a rectangle marked in Fig. 7), with uranium concentrations (wt.%) in selected spots measured by SEM/EDX.

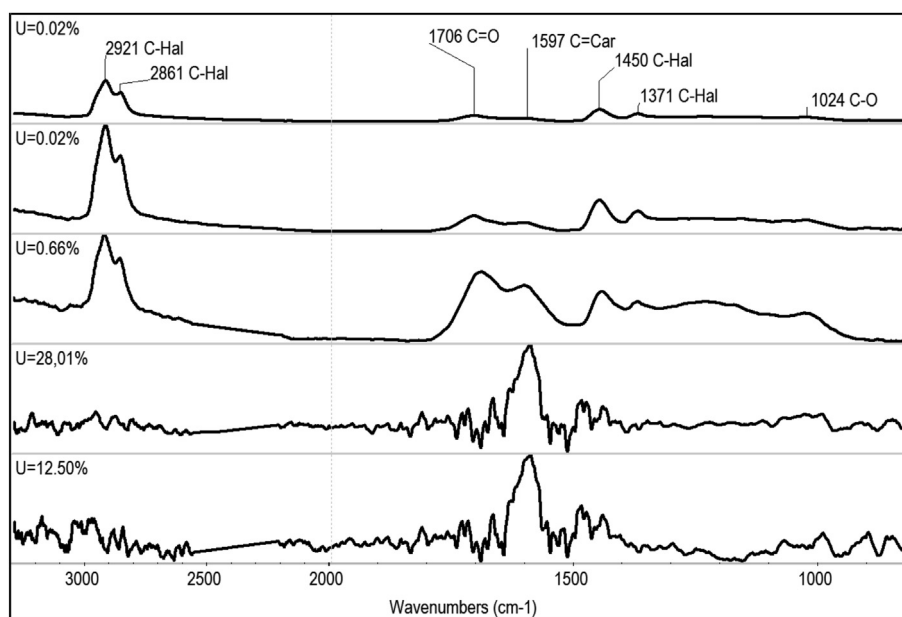


Fig. 9. Infrared microspectra obtained on a polished section from the Křižany amber in spots with various uranium concentrations (see Fig. 8; scanned area $30 \times 20 \mu\text{m}$ in each spot).

content - the amber from Nové Strašecí.

Uranium enrichment and the associated radiation affected the composition of the uraniferous amber by reducing the relative proportion of hydrogen, as indicated mainly by the H/C ratio, and in parallel, by decreasing the oxygen proportion (O/C ratio) in the bulk sample (see Table 1). A similar effect for the H/C ratio, but not for the O/C ratio, was observed for coal or kerogen (Havelcová et al., 2014b; Landais, 1996). This finding corresponds with results obtained in the bulk amber samples by infrared spectroscopy. The ATR-FTIR spectra (see Fig. 6) show that the Křižany amber has more

aromatic character and lower content of carbonyl and carboxyl groups than the amber from Nové Strašecí, which may point to dehydroaromatization and loss of the oxygen functional groups in the uraniferous sample. Quite a low level of exocyclic double bonds in the Nové Strašecí amber is a similar finding to that reported for Cenomanian fossil resins from other part of the Czech Republic - valchovite, neudorfite, and muckite. These resins also lacked the IR bands indicative of exocyclic methylene groups (Streibl et al., 1976), contrary to the IR spectra of the well-known Baltic amber of the Eocene-Oligocene age (Grimalt et al., 1988).

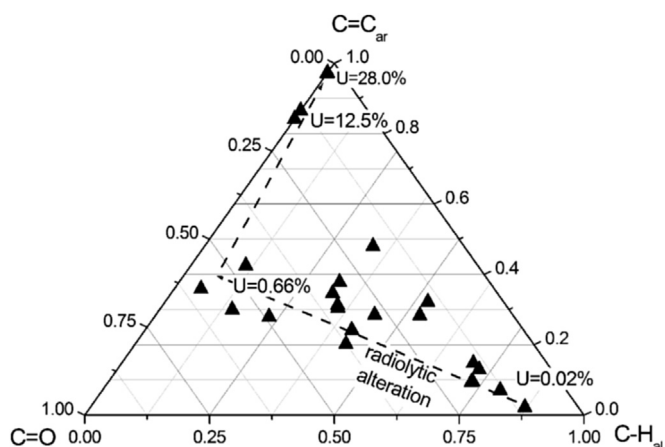


Fig. 10. Ternary diagram demonstrating changes in the relative abundance of aliphatic C–H bonds, carbonyl groups, and aromatic C=C bonds due to radiolytic alteration of the Křižany amber.

Changes in molecular structure of amber due to the presence of high levels of uranium were also indicated by thermogravimetric analysis. At 500 °C, less than half of the mass of the Křižany amber was combusted, whereas total combustion of the reference amber from Nové Strašecí was achieved below this temperature (see Fig. 5). These data indicate a high degree of polymerization, and

possible zonal graphitization of the Křižany uraniferous amber. Strong cross-linking of the amber structure was confirmed by very low yields of extraction with dichloromethane (see SOM in Table 1).

The uranium distribution within the Křižany amber was generally non-uniform and the anomalous enrichment was noted mainly in cracks. Microprobe analysis identified the Zr–Y–REE-enriched uraninite as the main mineral carrier of uranium (see Fig. 4 and Table 3), in agreement with prevailing mineral types in the whole NBCUOD. Micropetrographic evidence for radiolytic alteration in the uraniferous amber (see Fig. 2) was indicated by the morphologies and optical properties of resinite and ulminite. Around the uraninite-filled cracks, resinite changed to white haloes with reflectance reaching 0.35%, and its bright yellow fluorescence diminished and darkened in the haloes. Bright zones also appeared along cracks in huminite. Radiolytic alteration of ulminite was observed by its increased reflectance in the haloes and zones along the cracks. The size of the observed haloes corresponded to the estimated effective range of about 50 μm , within which the alpha particles have sufficient energy to alter organic matter (Sangély et al., 2007). The Nové Strašecí amber (see Fig. 3) also contained numerous cracks and hems at the edges of resinite grains, whose dark colour indicated weathering, in agreement with the high O/C ratio and higher content of oxygen-containing groups in the bulk sample.

Structural changes of organic matter in the uraniferous Křižany amber as a function of the local content of uranium were observed in detail (with a 30 μm resolution) by ATR-FTIR microspectroscopy

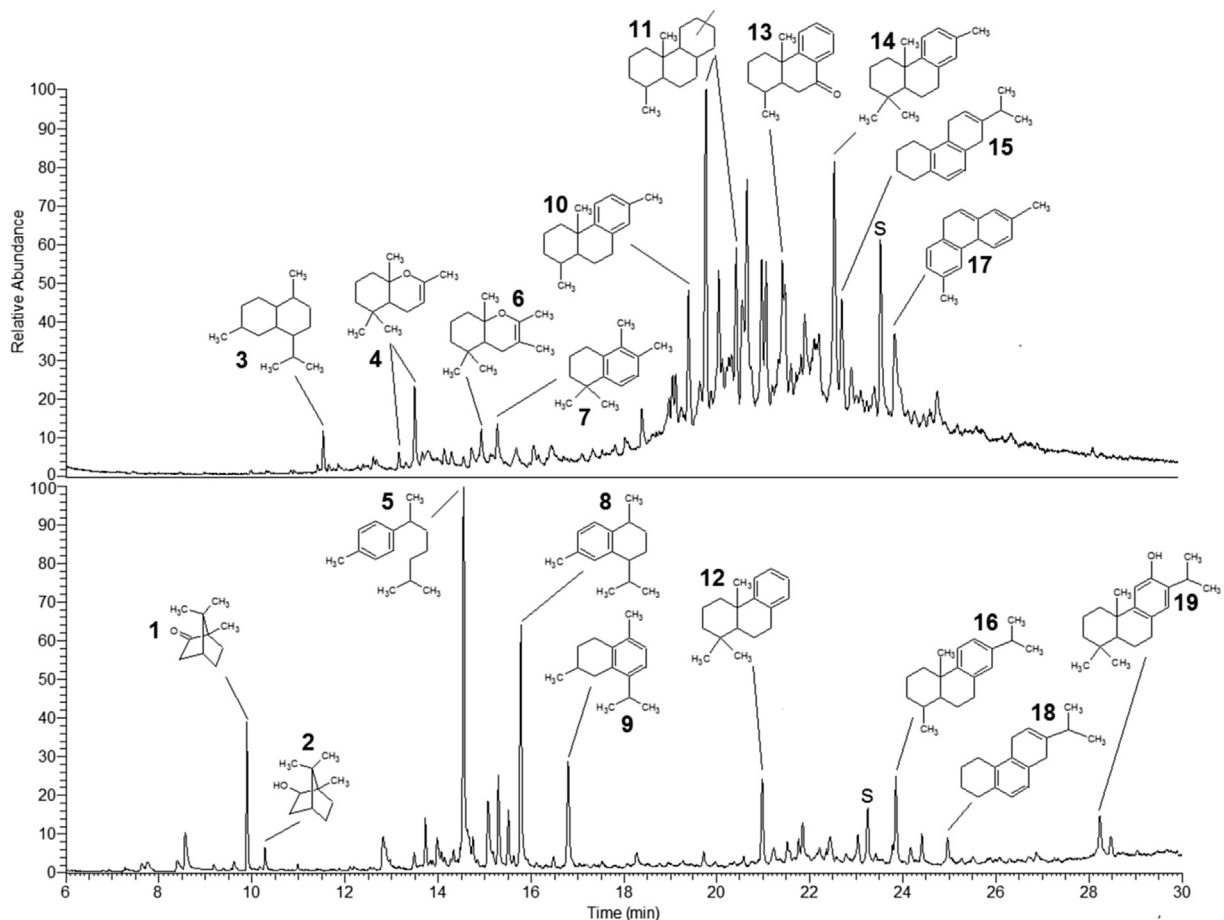


Fig. 11. Total ion chromatograms of extracts of amber samples from Křižany (top) and Nové Strašecí (bottom). The identified compounds are listed in Table 4. The numbers correspond to numbers in Table 4.

Table 4

Concentration of biomarkers identified in extracts of amber samples from Krížany and Nové Strašecí. The biomarker numbers identify their structural formulas shown in Fig. 11.

No.	Retention time (min)	Molecular weight	Formula	Compound name	Concentration (mg/g)	
					Křížany	Nové Strašecí
1	9.9	152	C ₁₀ H ₁₆ O	camphor		0.25
2	10.3	154	C ₁₀ H ₁₈ O	borneol		0.05
3	11.5	208	C ₁₅ H ₂₈	cadinane	0.07	
	12.8	160	C ₁₂ H ₁₆	dimethyltetraline		0.27
4	13.2	194	C ₁₃ H ₂₂ O	1a,2,5,5-teramethyl-cis-1a,4a,5,6,7,8-hexahydrochromene	0.03	
4	13.5	194	C ₁₃ H ₂₂ O	1a,2,5,5-teramethyl-trans-1a,4a,5,6,7,8-hexahydrochromene	0.18	
	13.7	204	C ₁₅ H ₂₄	sesquiterpene		0.13
	14.0	204	C ₁₅ H ₂₄	sesquiterpene		0.11
5	14.5	204	C ₁₅ H ₂₄	dihydro-ar-curcumene		1.36
6	14.9	208	C ₁₄ H ₂₄ O	4a,5,6,7,8,8a-hexahydro-2,3,5,5,8a-pentamethylchromene	0.08	
	15.1	202	C ₁₅ H ₂₂	sesquiterpene		0.30
7	15.3	188	C ₁₄ H ₂₀	methylionene	0.10	
	15.3	204	C ₁₅ H ₂₄	eudesmadiene		0.35
	15.5	202	C ₁₅ H ₂₂	cuparene		0.16
8	15.7	202	C ₁₅ H ₂₂	calamenene		1.37
	16.4	170	C ₁₃ H ₁₄	trimethylnaphthalene	0.10	
9	16.8	202	C ₁₅ H ₂₂	5,6,7,8-tetrahydrocadalene		0.51
10	19.4	228	C ₁₇ H ₂₄	16,17,19-trisnorabieta-8,11,13-triene	0.35	
11	19.8	248	C ₁₈ H ₃₂	C18 diterpene	0.77	
11	20.4	248	C ₁₈ H ₃₂	C18 diterpene	0.33	
	20.6	228	C ₁₇ H ₂₄	16,17,18-trisnorabieta-8,11,13-triene	0.29	
12	21.0	228	C ₁₇ H ₂₄	trimethyloctahydrophenanthrene		0.38
	21.1	262	C ₁₉ H ₃₄	C19 tricyclic terpane	0.35	
13	21.4	228	C ₁₇ H ₂₄	7-oxo-15-norpodocarpene	0.24	
	21.9	242	C ₁₈ H ₂₆	10,18-bisnorabieta-8,11,13-triene	0.19	
14	22.6	242	C ₁₈ H ₂₆	16,17-bisnordehydroabietane	0.34	0.14
15	22.7	224	C ₁₇ H ₂₀	18,19-bisnorsimonellite	0.26	
	23.6	256	C ₁₉ H ₂₈	18-norabieta-8,11,13-triene		0.10
16	23.9	270	C ₂₀ H ₃₀ O	dehydroabietane		0.31
	24.2	256	C ₁₉ H ₂₈	19-norabieta-8,11,13-triene		0.10
17	24.4	206	C ₁₆ H ₁₄	dimethylphenanthrene	0.31	
18	25.0	238	C ₁₈ H ₂₂	10,18-bisnorabieta-5,7,9(10),11,13-pentaene		0.12
19	28.3	286	C ₂₀ H ₃₀ O	L ferruginol		0.14

(see Figs. 7–10). This technique provided infrared spectra (Fig. 10) at various distances from uranium-containing mineral inclusions visualized by SEM-EDX (Fig. 7). Structural changes dependent on local concentrations of uranium can be observed in a 2D map constructed from the band intensities of aliphatic C–H bonds (Fig. 8), which shows that the radiolytic alteration occurred within a distance of 30–50 µm from the uranium-rich zones, in agreement with both the size of the observed haloes and the reported effective range of alpha radiation. Progress of the radiolytic alteration has been illustrated by a ternary diagram (Fig. 10) demonstrating changes in the relative abundance of aliphatic C–H bonds, carbonyl groups, and aromatic C=C bonds depending on the local uranium concentration. The results confirm that the radiolytic degradation of organic matter involves particularly dehydroaromatization of aliphatic cyclic hydrocarbons, which was almost complete in a spot containing 12.5 wt% of uranium, where aliphatic structures totally disappeared and the aromaticity approached unity. Such a high uranium level also caused cleavage of oxygen functional groups, which was almost complete at a spot with the highest uranium content of 28 wt%. Aromatic structures then prevailed in the amber structure. A similar trend was observed in uranium-rich bitumens (Sangély et al., 2007). The process of the severe radiolytic alteration of the amber and its resulting local structure also resembled carbonization behaviour of coal-tar pitch modified with rosin and formation of semi-cokes (Lin et al., 2009).

GC/MS (Fig. 11 and Table 4) and TMAH-Py–GC/MS (Fig. 12 and Table 5) analyses helped to identify a probable botanical source of the amber samples. Both samples were of the Cenomanian age, one of the warmest periods of the Phanerozoic that corresponds to one of the most important transgressive episodes of the geological record. The Cenomanian floras have been known for their diversity

(Nguyen Tu et al., 2002), exhibiting high diversification of angiosperms together with numerous gymnosperms. The presence of phenolic abietane (ferruginol) and specific sesquiterpenoids (e.g., cuparene) associated with Cupressaceae and Taxodiaceae families in the Nové Strašecí amber points to its probable origin in this group of conifers. A possible source of the uraniumiferous Křížany amber was difficult to pinpoint due to structural transformations induced by radiolytic alteration. The absence of plant triterpenoids and specific diterpenoids (such as ozic acid) in pyrograms eliminates the angiosperm plant family as a possible source, and the presence of sesqui- and diterpenoids suggests that both resins most likely arose from conifers.

In the uraniumiferous Křížany amber, both GC/MS and TMAH-Py–GC/MS analyses revealed structural transformations of terpenoids that are indicative of alterations, including defunctionalization and aromatization of resin. In natural systems, the effect of radiolytical alterations on a molecular level are identifiable by a reduction in the amount of isoprenoids versus *n*-alkanes, a decrease in long chain alkanes, an increase in aromaticity and an unusual distribution of aromatic hydrocarbons (Havelcová et al., 2014b; Dahl et al., 1988). However, the features based on alkane distribution cannot be used for amber samples because alkanes are not common components of their extracts. The only sign of alteration was an increased aromaticity of the identified set of diterpenoid compounds. The compounds were non-polymerizable abietane precursors without conjugated dienes. The Křížany amber had a significant UCM in the extract chromatogram as well as in the pyrogram, resulting from defunctionalization of resins and cross-linking of C–C bonds forming the three-dimensional hydrocarbon network.

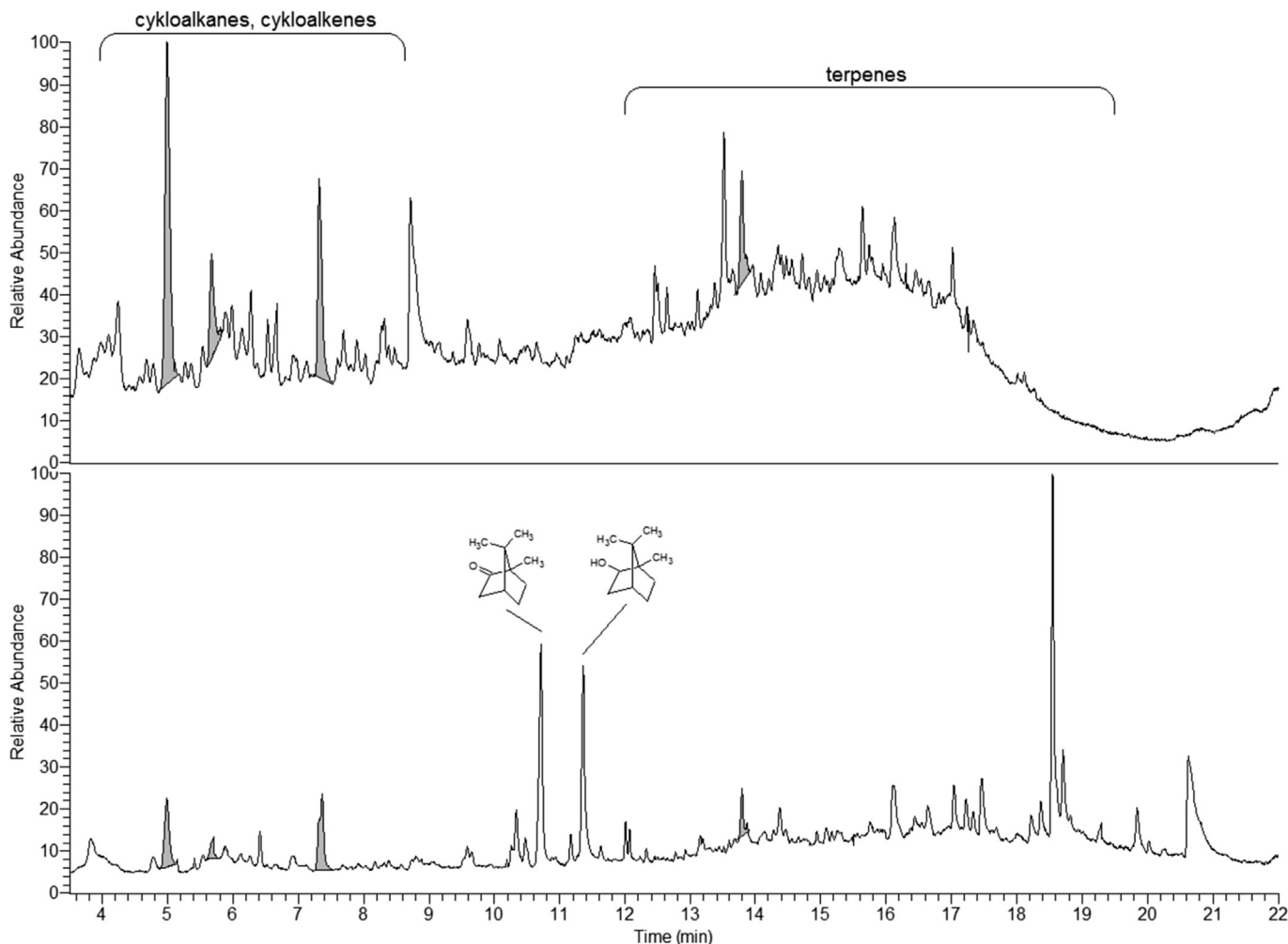


Fig. 12. Total ion pyrograms of amber samples from Krížany (top) and Nové Strašecí (bottom). Peaks of the compounds common for both resins are grey-filled. The identified compounds are listed in Table 4.

Table 5

Compounds identified in pyrograms of amber samples from Krížany and Nové Strašecí.

Retention time (min)	Molecular weight	Formula	Compound name	Krížany	Nové Strašecí
3.8	96	C ₇ H ₁₂	dimethylcyclopentene		x
4.2	112	C ₈ H ₁₆	dimethylcyclohexane	x	
4.8	108	C ₈ H ₁₂	dimethylcyclohexadiene		x
5.0	110	C ₈ H ₁₄	dimethylcyclohexene	x	x
5.6	124	C ₉ H ₁₆	tetramethylcyclopentene	x	x
7.3	124	C ₉ H ₁₆	tetramethylcyclopentene	x	x
8.7	120	C ₉ H ₁₂	trimethylbenzene	x	
10.3	154	C ₁₀ H ₁₈ O	fenchol		x
10.5	168	C ₁₁ H ₂₀ O	2-methoxy-1,7,7-trimethylbicyclo[2.2.1]heptane		x
10.7	152	C ₁₀ H ₁₆ O	camphor		x
11.2	154	C ₁₀ H ₁₈ O	borneol		x
13.5	208	C ₁₅ H ₂₈	cadinane isomer	x	
13.8	178	C ₁₃ H ₂₂	trimethyl-2-(2-methylcyclopropyl)-1-cyclohexene	x	x
15.6	166	C ₁₂ H ₂₂	1,2,3,6-tetramethylbicyclo[2.2.2]octane	x	
17.1	202	C ₁₅ H ₂₂	cadinatriene		x
17.2	204	C ₁₅ H ₂₄	eudesmadiene		x
17.5	202	C ₁₅ H ₂₆	cadinatriene		x
18.5	236	C ₁₇ H ₃₂	terpene		x
19.9	248	C ₁₈ H ₃₂	terpane		x
26.0	234	C ₁₈ H ₁₈	tetramethylphenanthrene		x

5. Conclusions

A multi-instrumental study of a unique sample of Cenomanian amber containing high amounts of uranium (almost 1.5 wt% on average) allowed us to describe structural changes in the amber caused by radiolytic alteration, which were observed in comparison with a reference amber of similar age and botanical origin, but not containing elevated amounts of uranium. The structural changes were observed on a microscale around micropores and cracks filled with uranium, mainly in the form Zr–Y-REE-enriched uraninite, but also on a macroscale in a bulk sample. The bulk radiolytic alteration involved an increase in the aromaticity due to dehydroaromatization of aliphatic cyclic hydrocarbons, defunctionalization (mainly loss of the oxygen functional groups), an increase in the degree of polymerization, cross-linking of C–C bonds, and formation of a three-dimensional hydrocarbon network. On a microscale, carbonization and zonal graphitization may have occurred around the uranium “hottest” spots.

Acknowledgements

This study was carried out thanks to the Operational Program Prague—Competitiveness, project “Centre for Texture Analysis” (No. CZ.2.16/3.1.00/21538), and the long-term conceptual development of the research organization RVO: 67985891. It was financially supported by Severočeské doly, a.s., and by the Czech Science Foundation grants No. 13-18482S and No. P108/12/G108.

References

- Anderson, K.B., Winans, R.E., Botto, R.E., 1992. The nature and fate of natural resins in the geosphere. II. Identification, classification, and nomenclature of resinite. *Org. Geochem.* 18, 829–841.
- Beck, C.W., Wilbur, E., Meret, S., 1964. Infra-red spectra and the origin of amber. *Nature* 4916, 256–257.
- Čadek, J., Mirovský, J., Novák, F., Vavřín, I., 1975. Association of uranium and zirconium in the sandstone type uranium deposits in northern Bohemia. *Čas. Mineral Geol.* 20, 131–140.
- Cebulak, S., Matuszewska, A., Langier-Kuzniarowa, A., 2003. Diversification of natural resins of various origin, oxyreactive thermal analysis and infrared spectroscopy. *J. Therm. Anal. Calorim.* 71, 905–914.
- Court, R.W., Sephton, M.A., Parnell, J., Gilmour, I., 2006. The alteration of organic matter in response to ionising irradiation: chemical trends and implications for extraterrestrial sample analysis. *Geochim. Cosmochim. Acta* 70, 1020–1039.
- Dahl, J., Hallberg, R., Kaplan, I.R., 1988. Effects of irradiation from uranium decay on extractable organic-matter in the Alum Shales of Sweden. *Org. Geochem.* 12, 559–571.
- Gough, M.A., Rowland, S.J., 1990. Characterization of unresolved complex mixtures of hydrocarbons in petroleum. *Nature* 344, 648–650.
- Grimál, J.O., Simoneit, B.R.T., Hatcher, P.G., Nissenbaum, A., 1988. The molecular composition of ambers. *Org. Geochem* 13, 677–690.
- Havelcová, M., Sýkorová, I., Mach, K., Dvořák, Z., 2014a. Organic geochemistry of fossil resins from the Czech Republic. *Procedia Earth Planet. Sci.* 10, 303–312.
- Havelcová, M., Machovič, V., Mizera, J., Sýkorová, I., Borecká, L., Kopecký, L., 2014b. A multi-instrumental geochemical study of anomalous uranium enrichment in coal. *J. Environ. Radioact.* 137, 52–63.
- ISO 7404-5, 2009. Methods for the Petrographic Analysis of Coals - Part 5: Method of Determining Microscopically the Reflectance of Vitrinite. International Organization for Standardization (ISO), Geneva.
- Jehlička, J., Jorge Villar, S.E., Edwards, H.G.M., 2004. Fourier transform Raman spectra of Czech and Moravian fossil resins from freshwater sediments. *J. Raman Spectrosc.* 35, 761–767.
- Kafka, J., 2003. Czech Ore and Uranium Mining Industry. Anagram, Ostrava. (in Czech).
- Kříbek, B., 1989. The role of organic matter in the metallogeny of the Bohemian Massif. *Econ. Geol.* 84, 1525–1540.
- Kříbek, B., Žák, K., Spangenberg, J., Jehlička, J., Prokeš, S., Komínek, J., 1999. Bitumens the late Variscan hydrothermal vein – type uranium deposit of Příbram, Czech Republic: sources, radiation - induced alteration, and relation to mineralization. *Econ. Geol.* 94, 1093–1114.
- Landais, P., 1996. Organic geochemistry of sedimentary uranium ore deposits. *Ore Geol. Rev.* 11, 33–51.
- Langenheim, J.H., 2003. *Plant Resins: Chemistry, Evolution, Ecology, and Ethnobotany*. Timber Press, Inc., pp. 141–194.
- Lin, Q., Su, W., Xie, Y., 2009. Effect of rosin to coal-tar pitch on carbonization behavior and optical texture of resultant semi-cokes. *J. Anal. Appl. Pyrolysis* 86, 8–13.
- McCready, A.J., Stumpfl, E.F., Melcher, F., 2003. U/Th-rich bitumen in Archean granites and Palaeoproterozoic metasediments, Rum Jungle Mineral Field, Australia: implications for mineralizing fluids. *Geofluids* 3, 147–159.
- Meunier, J.D., Landais, P., Pagel, M., 1990. Experimental evidence of uraninite formation from diagenesis of uranium-rich organic matter. *Geochim. Cosmochim. Acta* 54, 809–817.
- Mizera, J., Randa, Z., 2010. Instrumental neutron and photon activation analyses of selected geochemical reference materials. *J. Radioanal. Nucl. Chem.* 284, 157–163.
- Nakashima, S., Disnar, J.R., Perruchot, A., Trichet, J., 1984. Experimental study of mechanisms of fixation and reduction of uranium by sedimentary organic matter under diagenetic or hydrothermal conditions. *Geochim. Cosmochim. Acta* 48, 2321–2329.
- Nguyen Tu, T.T., Kvaček, J., Uličný, D., Bocherens, H., Mariotti, A., Broutin, J., 2002. Isotope reconstruction of plant palaeoecology. Case study of Cenomanian floras from Bohemia. *Palaeogeogr. Palaeoclimatol. Palaeoecol.* 183, 43–70.
- Otto, A., Wilde, V., 2001. Sesqui-, di-, and triterpenoids as chemosystematic markers in extant conifers – a review. *Bot. Rev.* 67, 141–238.
- Otto, A., Simoneit, B.R.T., Wilde, V., Kunzmann, L., Püttmann, W., 2002. Terpenoid composition of three fossil resins from Cretaceous and Tertiary conifers. *Rev. Palaeobot. Palynol.* 120, 203–215.
- Philp, R.P., 1985. *Fossil Fuel Biomarkers*. Elsevier, New York.
- Ragazzi, E., Roghi, G., Giaretta, A., Gianolla, P., 2003. Classification of amber based on thermal analysis. *Thermochim. Acta* 404, 43–54.
- Randa, Z., Frána, J., Mizera, J., Kučera, J., Novák, J.K., Ulrych, J., Belov, A.G., Maslov, O.D., 2007. Instrumental neutron and photon activation analysis in the geochemical study of phonolitic and trachytic rocks. *Geostand. Geoanal. Res.* 31, 275–283.
- Rodgers, K.A., Currie, S., 1999. A thermal analytical study of some modern and fossil resins from New Zealand. *Thermochim. Acta* 326, 143–149.
- Sangély, L., Chaussidon, M., Michels, R., Brouand, M., Cuney, M., Huault, V., Landais, P., 2007. Micrometer scale carbon isotopic study of bitumen associated with Athabasca uranium deposits: constraints on the genetic relationship with petroleum source-rocks and the abiogenic origin hypothesis. *Earth Planet. Sc. Lett.* 258, 378–396.
- Scharm, B., Burda, J., Hofreiter, V., Sulovský, P., Scharmová, M., 1980. Remarkable mineral assemblage on uranium deposits in northern Bohemia (the Stráž block). *Čas. Mineral Geol.* 25, 113–124.
- Scharmová, M., Scharm, B., 1994. Rhadophane group minerals in the uranium ore district of northern Bohemia (Czech Republic). *J. Czech Geol. Soc.* 39, 267–280.
- Shahin, H.A.A., 2014. Geochemical characteristics and chemical electron microprobe U-Pb-Th dating of pitchblende mineralization from Gabal Gattar Younger granite, North Eastern Desert, Egypt. *Open J. Geol.* 4, 24–32.
- Smetana, R., Mužák, J., Novák, J., 2002. Environmental impact of uranium ISL in northern Bohemia. In: Merkel, B.J., Planer-Friedrich, B., Wolkersdorfer, C. (Eds.), *Uranium in the Aquatic Environment*. Springer-Verlag, Berlin, Heidelberg, pp. 703–712.
- Streibl, M., Vašíčková, S., Herout, V., Bouška, V., 1976. Chemical composition of Cenomanian fossil resins from Moravia. *Coll. Czechoslov. Chem. Commun.* 41, 3138–3145.
- Sulovský, P., 2005. Sandstone-hosted U-zr-REE Mineralization in North Bohemian Cretaceous Basin. *Uranium Production and Raw Materials for the Nuclear Fuel Cycle*. IAEA, Vienna, pp. 91–95.
- Sýkorová, I., Pickel, W., Christianis, K., Wolf, M., Taylor, G.H., Flores, D., 2005. Classification of huminite – ICCP system 1994. *Int. J. Coal Geol.* 62, 85–106.
- Taylor, G.H., Teichmüller, M., Davis, A., Diessel, C.F.K., Littke, R., Robert, P., 1998. *Organic Petrology*. Gebrüder Borntraeger, Berlin-Stuttgart.
- Trevisani, E., Papazzoni, C.A., Ragazzi, E., Roghi, G., 2005. Early Eocene amber from the the “Pesciara di Bolca” (Lessini Mountains, Northern Italy). *Palaeogeogr. Palaeoclim.* 223, 260–274.
- Vávra, N., 1993. Chemical characterization of fossil resins (‘amber’)—a critical review of methods, problems and possibilities: determination of mineral species, botanical sources and geographical attribution. *Abh. Geol. B. A* 49, 147–157.
- von Rudloff, E., Hogge, L., Granat, M., 1980. The leaf oil terpene composition of *Juniperus occidentalis*. *Phytochemistry* 19, 1701–1703.
- Zhao, D., Ewing, R.C., 2000. Alteration products of uraninite from the Colorado Plateau. *Radiochim. Acta* 88, 739–750.